RSC Advances

PAPER

View Article Online
View Journal | View Issue

Cite this: *RSC Adv.*, 2026, **16**, 15764

Aryldiazonium-grafted bamboo-derived activated carbon: a solid acid catalyst with stable C–C bonded sulfonic acid sites for biodiesel production *via* esterification

Xiaona Wang,[a] Bingxin Zhang, *[b] Zilin Hu,[b] Pan Zhao[c] and Qunhui Wang [a]

This study proposes a robust carbon-based solid acid catalyst (ACC600) prepared from bamboo waste for efficient biodiesel production *via* esterification. The catalyst was synthesised through phosphoric acid activation, followed by pyrolysis at 600 °C and subsequent functionalisation with sulfonic acid groups using an aryldiazonium sulfonation strategy. Under optimal conditions, ACC600 showed a high sulfonic acid density (1.295 mmol g^{-1}) and a well-developed porous structure. It exhibited excellent catalytic performance in the esterification of oleic acid, achieving 97.5% conversion under mild reaction conditions. Notably, ACC600 exhibited outstanding stability, maintaining 79.0% of its initial activity after 10 consecutive reuses, which was attributed to its rigid carbon framework effectively suppressing the leaching of active sites. The catalyst also showed promising results when applied to real-world soybean saponin acidified oil, confirming its potential for practical industrial application. This work provides a viable approach for designing highly stable solid acid catalysts from biomass for sustainable biofuel production.

Received 30th December 2025
Accepted 13th March 2026

DOI: 10.1039/d5ra10105k

rsc.li/rsc-advances

1 Introduction

With the continuous growth of global energy demand and the increasing severity of environmental issues caused by fossil fuel consumption, the development of renewable and clean alternative energy has become one of the critical research directions in contemporary science.[1] Biodiesel, consisting of monoalkyl esters of fatty acids produced through the transesterification or esterification of animal/vegetable oils or waste oils with short-chain alcohols (*e.g.* methanol),[2] is recognised as an ideal substitute for traditional petroleum-based diesel owing to its biodegradability, non-toxicity and low emission of combustion pollutants.[3]

However, the commercial production of biodiesel is still plagued by its excessively high cost.[4] To reduce production expenses, low-cost waste oils with high acid values (waste cooking oil and soapstock acidified oil) have been used as raw materials.[5] For the conversion of high-concentration free fatty acids (FFAs) in such feedstocks, solid acid-catalysed esterification is considered a superior alternative to conventional liquid acid-catalysed esterification. Its advantages lie in the ease of product separation, reusability and environmental friendliness.[6,7] Among various solid acid catalysts, carbon-based variants have garnered extensive research attention because of the wide availability of raw materials, large specific surface area and tunable surface chemical properties.[8] Nevertheless, these catalysts generally suffer from a critical bottleneck in practical applications: insufficient catalytic stability, particularly the rapid leaching of active sites in liquid-phase reaction systems.[9]

This stability limitation primarily stems from the inherent drawbacks of traditional preparation methods. Currently, most carbon-based solid acid catalysts are fabricated *via* direct sulfonation with concentrated sulfuric acid or fuming sulfuric acid.[10,11] Although this method is straightforward and can effectively introduce sulfonic acid groups (–SO_3H), the harsh oxidising reaction environment leads to excessive oxidation and hydrolysis of the carbon framework.[12] Most of the sulfonic acid groups formed *via* this method are bonded to the carbon skeleton through C–O–SO_3H linkages.[13] Such C–O bonds exhibit poor chemical stability in the hydrothermal environment of esterification reactions and are prone to hydrolytic cleavage, which results in the detachment of sulfonic acid groups from the support into the reaction liquid phase and the irreversible loss of catalytically active sites.[14,15]

In addition, traditional sulfonation suffers from poor selectivity, often accompanied by the formation of various inactive sulfur-containing by-products (sulfones and sulfonic esters).[16]

[a]*Department of Environmental Science and Engineering, School of Energy and Environmental Engineering, University of Science and Technology Beijing, 30 Xueyuan Road, Haidian District, Beijing 100083, China*

[b]*China Coal Research Institute Co. Ltd, Beijing 100013, China. E-mail: 18401619821@163.com; Fax: +86-18401619821; Tel: +86-18401619821*

[c]*Department of Environmental Engineering, Tianjin College, University of Science and Technology Beijing, Tianjin 301830, China*

This reduces the density of effective acid sites and may also block catalyst pores and impair mass transfer efficiency.[17] Additionally, carbon supports obtained through direct biomass carbonisation have limited mechanical strength and structural rigidity, and are susceptible to pore structure collapse and physical damage during repeated use, which further accelerates the loss of active components.[18] Therefore, it is crucial to refine sulfonation strategies for realising more stable chemical bonding between sulfonic acid groups and carbon supports.

Thus, in this study, we employed an aryldiazonium sulfonation strategy to covalently graft sulfonic acid groups onto bamboo-derived activated carbon through stable C–C bonds. Compared to conventional C–O–SO_3H linkages formed by direct sulfonation, these C–C bonds exhibit higher chemical and hydrothermal stability, effectively resisting hydrolysis and detachment during esterification reactions. Mechanistically, the aryldiazonium reaction selectively generates aryl radicals that covalently bind to sp^2-hybridized carbon sites on the activated carbon surface, anchoring –SO_3H groups as stable active sites. Coupled with the high surface area and rigid framework of bamboo-based carbon, this approach prevents pore collapse and ensures even dispersion of active sites, thereby suppressing leaching and maintaining catalytic performance over repeated cycles. This strategy provides a dual advantage: chemically stable active sites and physically robust support, addressing the key stability bottleneck of carbon-based solid acid catalysts. The properties, catalytic performance and stability of the catalyst in esterification reactions were systematically investigated, focusing on the mechanism underlying its enhanced stability. The present work aimed to provide new insights and approaches for addressing the stability bottleneck of carbon-based solid acid catalysts.

2 Experimental

2.1 Materials

Agricultural bamboo waste collected from Guangxi, China, was used as the raw material. It was crushed using a pulveriser, sieved through a 0.45 mm mesh, dried in an air blast drying oven and stored in sealed containers for subsequent use. Soybean saponin acidified oil was obtained from a local factory in Guangxi, with its fatty acid content provided in Table 1. Based on the types and mass fractions of fatty acids, the average relative molecular mass of the soybean saponin acidified oil was calculated to be approximately 280.02 g mol^{-1}. Additionally, the acid and saponification values of the oil, determined through titration, were 126.26 and 171.40 mg KOH per g, respectively.

Table 1 Fatty acid composition of soybean saponin acidified oil

Fatty acid	Simplified	Content (wt%)
Palmitic acid	C16:0	5.71
Stearic acid	C18:0	1.88
Trans-oleic acid	C18:1n9t	1.02
Oleic acid	C18:1n9c	39.40
Linoleic acid	C18:2n6c	44.69
α-Linolenic acid	C18:3n3	5.36

All chemical reagents, including methanol, *p*-aminobenzenesulfonic acid, phosphoric acid, potassium hydroxide and sodium nitrite, were of analytical grade, purchased from Sinopharm Chemical Reagent Beijing.

2.2 Catalyst preparation

The activated carbon-based solid acid catalyst was prepared as follows. First, 15 g of biomass powder was placed in a crucible and impregnated with 50 wt% phosphoric acid at a solid-to-liquid ratio of 1 : 1 for 12 h. The crucible was then transferred to a muffle furnace and heated to a predetermined temperature (500 °C, 600 °C or 700 °C) at a heating rate of 3 °C min^{-1} under a nitrogen atmosphere, followed by pyrolysis for 3 h. After cooling to room temperature, the resulting solid was transferred to a beaker and repeatedly washed with deionised water. The mixture was vacuum-filtered to remove residual inorganic components, after which the obtained solid was dried in an oven at 105 °C to a constant weight, yielding phosphoric acid-activated carbon, designated as AC*x* (where *x* is the pyrolysis temperature).

Subsequently, 5 mL of concentrated hydrochloric acid was added to a beaker containing 100 mL of deionised water, followed by the addition of a certain amount of *p*-aminobenzenesulfonic acid and magnetic stirring in an ice-water bath. After some time, sodium nitrite (at a mass ratio of 1 : 2 to *p*-aminobenzenesulfonic acid) was added to the mixture, followed by additional stirring for 1 h. The mixture was then filtered under suction, and the resulting white solid (4-benzenediazonium sulfonate) was washed with deionised water. The obtained white solid was dispersed in 100 mL of 50% ethanol, and 1 g of the previously prepared activated carbon was added to the dispersion, followed by magnetic stirring in an ice-water bath for a specific duration. After the reaction, the mixture was filtered and thoroughly rinsed with deionised water until no residual white solid was observed. The resulting solid was dried in an oven at 105 °C to a constant weight to remove residual moisture, with the final catalyst denoted as ACC*x* (where *x* is the pyrolysis temperature).

To optimize the sulfonation conditions, a series of catalysts were prepared by varying the mass ratio of *p*-aminobenzenesulfonic acid to activated carbon (6 : 1, 8 : 1, 10 : 1, 12 : 1) while fixing the sulfonation time at 6 h, and by varying the sulfonation time (2, 4, 6, 8 h) at the optimal mass ratio of 10 : 1. All other steps remained identical to those described above. The sulfonic acid density of the resulting catalysts was determined by acid–base titration.

2.3 Esterification experiments and catalyst reuse

Esterification reactions were performed in a 250 mL round-bottom flask equipped with a reflux condenser and a magnetic stirrer, which was placed in a thermostatically controlled water bath. The water bath was first heated to the preset temperature, and then the flask containing oil, methanol and catalyst was placed in the water bath to initiate the

esterification reaction. The reaction conditions were as follows: 30 g of oil, catalyst dosage of 2–10 wt% (based on the mass of oil), methanol-to-oleic acid molar ratio from 4 : 1 to 12 : 1, reaction time of 2–10 h and reaction temperature of 45–85 °C. After the reaction, the flask was removed and allowed to stand for 30 min, after which excess methanol was decanted. A small amount of the remaining product was sampled to determine the acid value. The esterification product was titrated with a KOH–ethanol solution, and the acid value and FFA conversion were calculated using eqn (1) and (2), respectively:[19]

$$\text{Acid value} = \frac{V \times c \times 56.11\ \text{g mol}^{-1}}{m} \quad (1)$$

where V is the volume of the KOH solution used, c is the concentration of the KOH solution, 56.11 g mol^{-1} is the molar mass of KOH and m is the mass of the sample.

$$\text{Conversion}(\%) = \frac{\text{AV}_\text{i} - \text{AV}_\text{f}}{\text{AV}_\text{i}} \times 100\% \quad (2)$$

where AV_i is the initial acid value of the reactant, and AV_f is the final acid value of the product. The calculations were conducted in triplicate, and the average values were obtained.

After each esterification reaction, the catalyst was separated from the product *via* centrifugation. The recovered catalyst was repeatedly washed with *n*-hexane and anhydrous ethanol, filtered and dried at 105 °C for 12 h to a constant weight. The regenerated catalyst was reused in subsequent esterification reactions following the same procedure as in the first run.

2.4 Analytical methods

The functional groups in the catalyst structure were investigated using Fourier transform infrared spectroscopy (NICOLET iS10, Thermo Fisher Scientific) at a resolution of 4 cm^{-1} and scanning range of 400–4000 cm^{-1}. The phase structure of the samples was analysed through X-ray diffraction (XRD; Ultima IV, Rigaku). The micromorphology of the samples was observed *via* scanning electron microscopy (SEM; Gemini 300, ZEISS). Elemental analysis (EA; Elementar, Germany) of C, H, N, and S was performed using a Vario EL III elemental analyzer to quantify the total sulfur content and verify the loading of sulfonic acid groups. The N_2 adsorption–desorption isotherms of the samples were measured using a Micromeritics ASAP 2460 automatic specific surface area and porosity analyser with high-purity N_2 as the adsorption medium and liquid nitrogen (77 K) as the cold trap. The thermal decomposition of the samples was investigated through simultaneous thermal analysis using a PerkinElmer STA-8000 analyser. The chemical states of elements on the catalyst surface were characterised *via* X-ray photoelectron spectroscopy (XPS; ESCALAB 250Xi, Thermo Fisher Scientific). The sulfonic acid density of the catalyst was determined using acid–base titration.[20] Specifically, 0.5 g of the catalyst was mixed with 50 mL of 2 M NaCl solution in a centrifuge tube and shaken for 6 h. After filtration, 20 mL of the filtrate was transferred to a different vessel, a few drops of phenolphthalein indicator were added and the solution was titrated to neutrality with 0.05 M NaOH solution. The quantification of various sulfonic acids described in Section 3.4 was conducted using methods reported in our previous study.[21]

3 Results and discussion

3.1 Optimisation of ACC preparation conditions

The preparation temperature of activated carbon is a key factor affecting its specific surface area and structural rigidity. To clarify this effect, the acid density of activated carbon catalysts prepared at different temperatures was investigated under at a mass ratio of *p*-aminobenzenesulfonic acid-to-activated carbon of 10 : 1 and sulfonation time of 6 h.

As shown in Fig. 1, with the increase in pyrolysis temperature, the acid density and specific surface area of the catalyst first increased and then decreased, with the catalyst prepared at 600 °C exhibiting the highest sulfonic acid density (1.295 mmol g^{-1}) and total acid density (2.053 mmol g^{-1}). This was attributed to the fact that at low carbonisation temperatures, the insufficient porosity of activated carbon restricts the contact between aryldiazonium sulfonate and the carbon material;[22] at the same time, at excessively high temperatures, the enhanced rigidity of activated carbon reduces the number of active sites available for the grafting of benzenesulfonic acid radicals, leading to reduced sulfonic acid density.[23] Therefore, 600 °C was selected as the optimal pyrolysis temperature for the preparation of activated carbon-based solid acid catalysts.

To efficiently screen the key sulfonation parameters, the effects of sulfonation time and the mass ratio of *p*-aminobenzenesulfonic acid-to-activated carbon were investigated. A series of catalysts was prepared using activated carbon obtained at 600 °C under different sulfonation conditions, and their sulfonic acid densities were measured (Table 2). At a sulfonation time of 6 h, the sulfonic acid density of the catalyst gradually increased with the dosage of *p*-aminobenzenesulfonic acid, reaching a maximum of 1.295 mmol g^{-1} at a mass ratio of 10 : 1. However, further increasing the dosage of *p*-aminobenzenesulfonic acid only led to a slight increase in sulfonic acid density because the amount of sulfonating agent

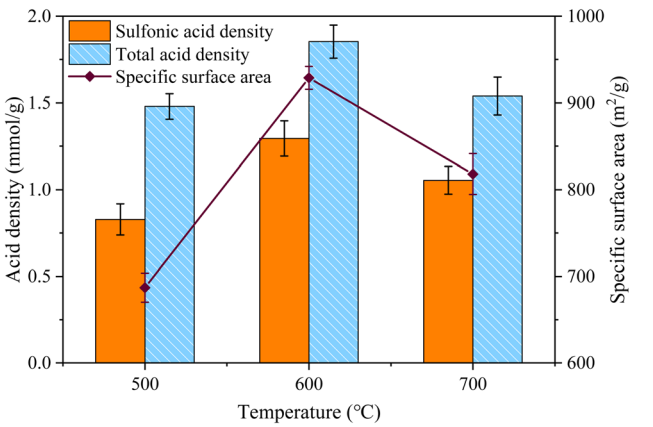

Fig. 1 Acid density and specific surface area of activated carbon-based solid acid catalysts prepared at different carbonisation temperatures.

Table 2 Sulfonic acid density of activated carbon-based solid acid catalysts prepared under different sulfonation conditions

Para-aminobenzenesulfonic acid/ activated carbon (w : w)[a]	Sulfonic acid density (mmol g^{-1})	Sulfonation time (h)[b]	Sulfonic acid density (mmol g^{-1})
6 : 1	0.894	2	0.738
8 : 1	1.076	4	0.986
10 : 1	1.295	6	1.295
12 : 1	1.303	8	1.310

[a] Sulfonation time fixed at 6 h. [b] *Para*-aminobenzenesulfonic acid/AC mass ratio fixed at 10 : 1.

was already sufficient for the sulfonation of activated carbon at this ratio. Moreover, excessive sulfonating agents may undergo side reactions, which is unfavourable for the loading of sulfonic acid groups.

At a mass ratio of *p*-aminobenzenesulfonic acid-to-activated carbon of 10 : 1, sulfonic acid density showed a positive correlation with sulfonation time. However, when the reaction time exceeded 6 h, the loading of sulfonic acid groups reached the

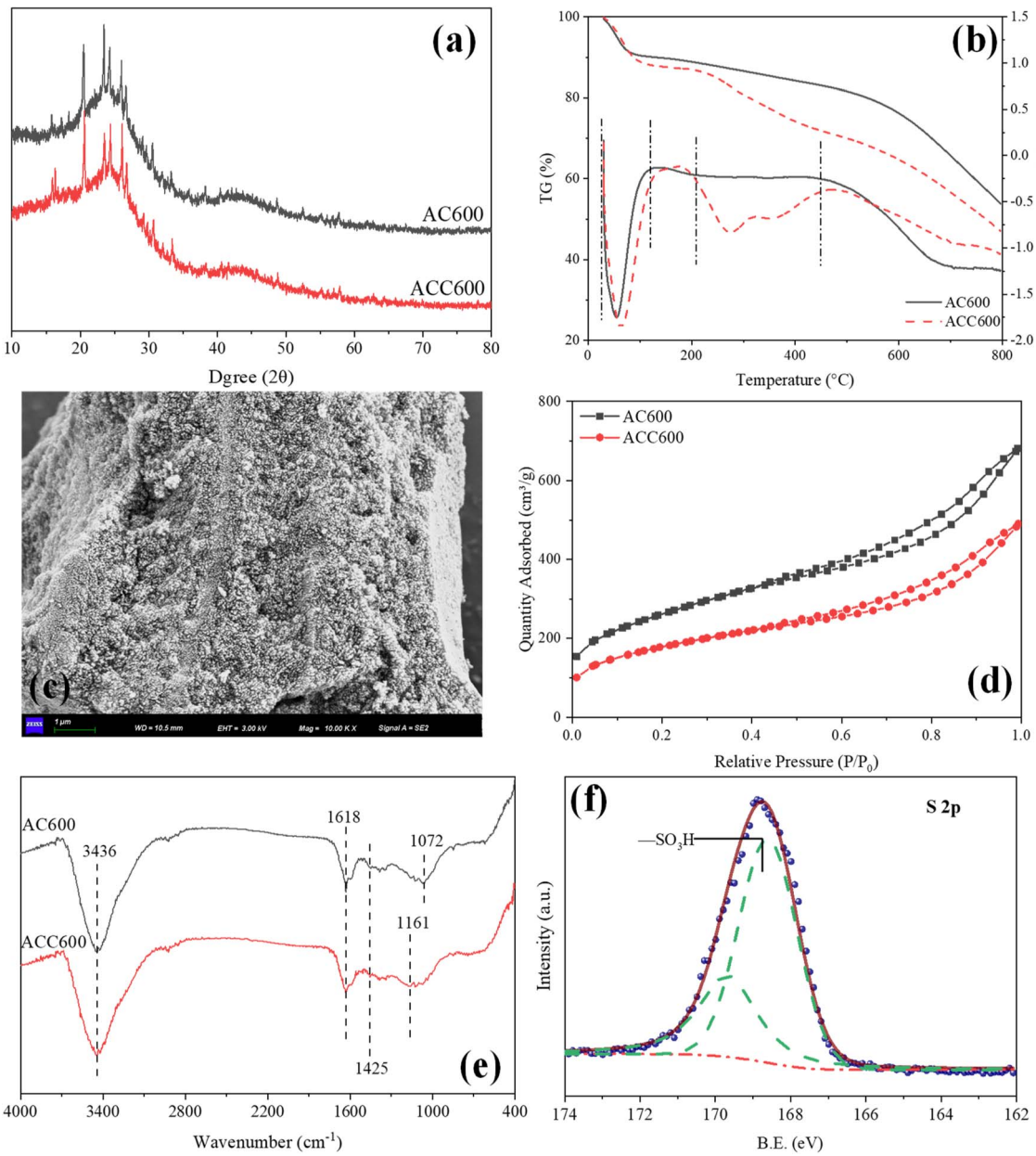

Fig. 2 Characterisation of AC600 and ACC600. (a) XRD patterns, (b) TG and DTG curves, (c) SEM images, (d) nitrogen adsorption–desorption curves, (e) FT-IR spectras, (f) XPS spectras.

Table 3 Pore structure and elemental analysis of AC600 and ACC600

Sample	Specific surface area ($m^2\ g^{-1}$)	Pore volume ($cm^3\ g^{-1}$)	Pore diameter (nm)	C (%)	H (%)	O (%)	N (%)	S (%)
AC600	929	1.00	5.16	54.52	4.34	40.77	0.09	0.19
ACC600	627	0.71	5.57	55.08	4.07	36.65	0.08	4.22

upper limit, with the further extension of the reaction time resulting only in a slight increase in sulfonic acid density. Thus, the optimal sulfonation conditions were determined as a *p*-aminobenzenesulfonic acid-to-activated carbon mass ratio of 10 : 1 and a sulfonation time of 6 h.

3.2 Characterisation of catalysts

To elucidate the physicochemical properties of activated carbon and the catalyst, comprehensive characterisation was conducted. Fig. 2a shows the XRD patterns of AC600 and ACC600. Both samples exhibit a broad characteristic peak in the 2θ range of 15–35°, which corresponds to the (002) diffraction peak, indicating the parallel orientation and ordering degree of aromatic layers in the crystals. A weak characteristic peak observed at 2θ = 40–50° was assigned to the (101) diffraction peak, suggesting the presence of amorphous carbon with a low content of randomly arranged crystalline graphite.[24] The similar XRD patterns of the two samples indicate that their carbonised structures do not considerably differ, implying that sulfonation with aryldiazonium sulfonate did not damage the microstructure of activated carbon.

The thermogravimetric curves of AC600 and ACC600 are presented in Fig. 2b. Both samples show a slight weight loss (<12 wt%) below 110 °C, which was attributed to the desorption of adsorbed water. With the further increase in temperature, the masses of both materials decrease to varying degrees. According to the derivative thermogravimetric curves, the mass loss rate of AC600 is relatively constant in the temperature range of 150–500 °C, with the thermogravimetric curve showing that the mass loss in this stage, caused by the decomposition of oxygen-containing groups in activated carbon, is relatively low (<5 wt%).[25] In contrast, ACC600 exhibits a mass loss of nearly 15 wt% in the range of 200–450 °C owing to the decomposition of the sulfonic acid groups successfully loaded on its surface.[26] When the temperature exceeds 600 °C, the mass loss rate of both materials considerably increases because of the decomposition of the carbon material itself at temperatures exceeding the preparation temperature. The SEM image of ACC600 is shown in Fig. 2c, indicating a dense and fine pore structure. Such a structure facilitates the diffusion of reactants (FFAs and methanol) and products within the catalyst.

Fig. 2d shows the N_2 adsorption–desorption isotherms of AC600 and ACC600 under a nitrogen atmosphere. The isotherms of both materials are type II curves according to the BDDT classification, indicating multilayer adsorption on the nonporous surface.[27] A clear hysteresis loop is observed in the relative pressure range of P/P_0 = 0.45–0.99, confirming the presence of mesopores.[28] The pore structure parameters of AC600 and ACC600 are summarised in Table 3. AC600 has a specific surface area of 929 $m^2\ g^{-1}$ and a pore volume of 1.00 $cm^3\ g^{-1}$, indicating that bamboo was successfully converted to activated carbon with abundant pores *via* phosphoric acid impregnation, which is favourable for the loading of arylsulfonic acid groups ($PhSO_3H$). After arylation, the specific surface area and pore volume of the catalyst decrease by 32% and 29%, respectively, indicating that $PhSO_3H$ groups were successfully anchored on the activated carbon and partially occupied or blocked the pores in the carbon material.

In addition, the surface functional groups of AC600 and ACC600 were analysed using Fourier transform infrared spectroscopy (Fig. 2e). Both samples exhibit a strong absorption peak at 3436 cm^{-1}, which corresponds to the stretching vibrations of O–H, indicating the presence of adsorbed water or carboxyl groups. The peaks at 1618 and 1425 cm^{-1} were attributed to the stretching vibrations of C=C and CH_2, respectively, suggesting the presence of aromatic compounds.[29] The absorption peak of AC600 at 1072 cm^{-1} is related to the asymmetric stretching of C–O–C. At the same time, the absorption peak of ACC600 at 1072 cm^{-1} is notably weaker, with a new characteristic peak appearing at 1161 cm^{-1}, which originates from the symmetric stretching of $-SO_3H$.[30] This implies that the original C–O–C linkages were broken during the aryl sulfonation, enabling the tight bonding of arylsulfonic acid groups with the carbon material.

The chemical states of sulfur-containing functional groups in ACC600 were analysed using XPS (Fig. 2f). In the S 2p spectrum, the peaks at 168.6 and 169.78 eV indicate the presence of $-SO_3H$ groups, suggesting that sulfonation with aryldiazonium sulfonate only introduced sulfonic acid groups into the carbon material.[31] The exclusive presence of $-SO_3H$ species in the S 2p spectrum and the weakening of the C–O–C peak in FTIR (Fig. 2e) indicate that sulfonic acid groups are grafted *via* C–C bonds rather than through oxygen linkages. This is consistent with the aryldiazonium reaction mechanism, where aryl radicals covalently bind to sp^2-hybridized carbon sites on the activated carbon surface.[32] In contrast to direct sulfonation with concentrated sulfuric acid, which induces various oxidation reactions and generates multiple sulfur-containing functional groups, the proposed sulfonation route features a single reaction pathway, allowing for more precise regulation of the loading of sulfonic acid groups.

Finally, the elemental analysis was conducted to quantify the sulfur content and corroborate the acid–base titration results (Table 3). The sulfur content of ACC600 increased by 4.03 wt% compared to AC600, corresponding to a sulfonic acid density of approximately 1.26 mmol g^{-1}, which is in excellent agreement with the titration value of 1.295 mmol g^{-1}. This consistency

confirms the reliability of the titration method and indicates that the majority of sulfur species are present as $-SO_3H$ groups. Furthermore, the absence of increased nitrogen in the EA results indicates that the diazotization reaction proceeded in a pure manner, without generating residual amines or azo byproducts.

3.3 Optimisation of esterification reaction conditions

To evaluate the catalytic activity of ACC600, it was employed as a catalyst in the esterification of oleic acid with methanol, and the reaction conditions were optimised.

The effect of catalyst loading on the conversion was investigated at a methanol/oil molar ratio of 6 : 1, reaction temperature of 65 °C and reaction time of 6 h. As shown in Fig. 3a, the conversion is only 83.5% when at a catalyst loading of 2 wt%, but gradually increases with the catalyst dosage. With an increase in catalyst loading from 4 to 6 wt%, the conversion increases from 89.9% to 92.9%. However, further increases in the catalyst loading lead to only a slight improvement in the conversion because the number of catalytically active sites is already excessive at 6 wt%.[33] Therefore, the catalyst loading of 6 wt% was selected for subsequent experiments.

The effect of the methanol/oil molar ratio on the conversion was studied at a catalyst loading of 6 wt%, reaction temperature of 75 °C and reaction time of 6 h. The results in Fig. 3b show that under these conditions, the conversion reaches 92.9% at a methanol/oil molar ratio of 6 : 1, with a further increase in the molar ratio resulting only in a minor increase in the conversion. This was attributed to the excess methanol diluting the volume concentration of oleic acid and the catalyst, thereby reducing the collision frequency between oleic acid molecules and the active sites of the catalyst.[34] Thus, 6 : 1 was considered the optimal methanol/oil molar ratio.

Subsequently, the effect of reaction temperature on the conversion was explored at a catalyst loading of 6 wt%, a methanol/oil molar ratio of 6 : 1 and a reaction time of 6 h. As shown in Fig. 3c, increases in reaction temperature promote the esterification reaction. The conversion of oleic acid is only 78.0% at 45 °C but increases to 97.5% at 75 °C. When the temperature exceeds 85 °C, the conversion no longer increases because the reaction becomes more intense, and a large amount of methanol turns into gas (the boiling point of methanol is 64.7 °C), leading to a decrease in the concentration of methanol directly participating in the liquid-phase reaction.[35] Therefore, 75 °C was chosen as the optimal reaction temperature.

The effect of reaction time on the conversion was examined at a catalyst loading of 6 wt%, a methanol/oil molar ratio of 6 : 1 and a reaction temperature of 75 °C. Fig. 3d shows that the conversion reaches 97.5% at a reaction time of 6 h and remains

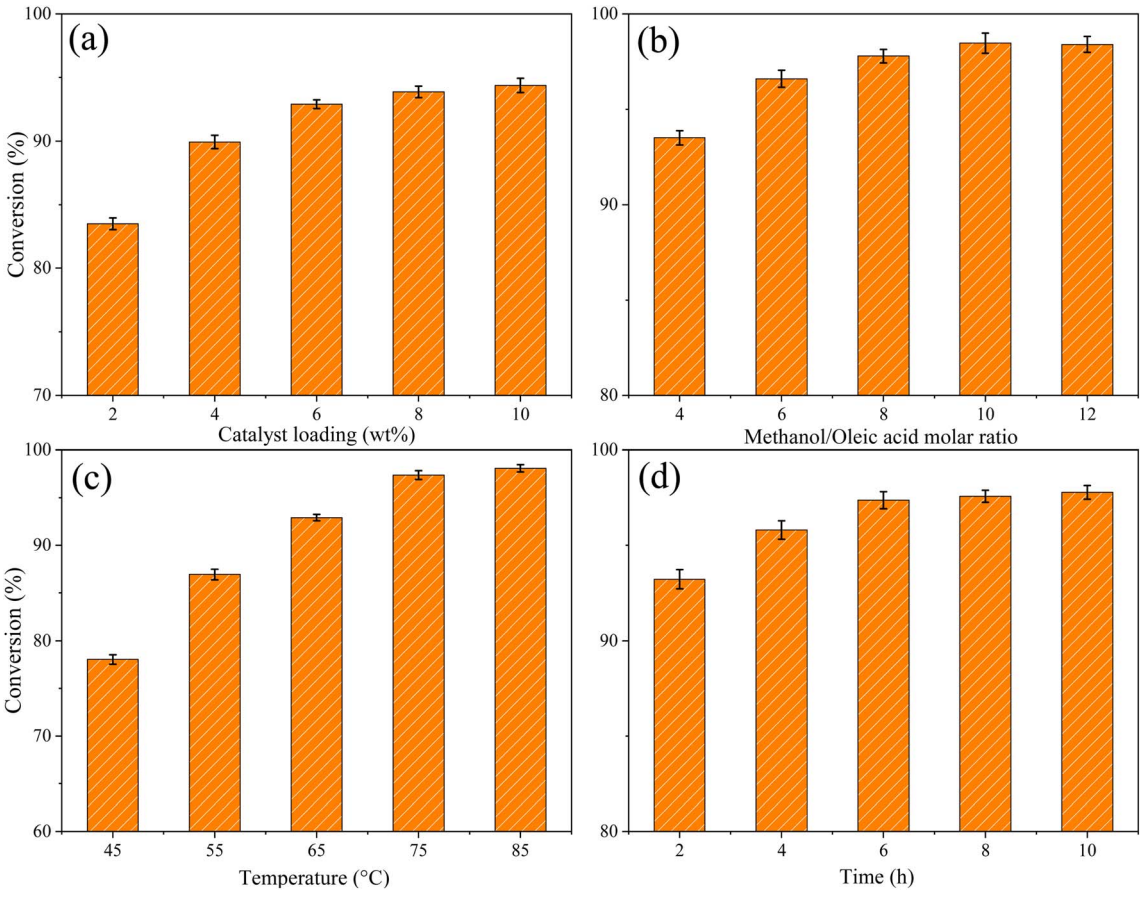

Fig. 3 Effects of different parameters on the esterification reaction: (a) catalyst loading, (b) methanol/oil molar ratio, (c) temperature and (d) time.

stable with its further extension, indicating that the reaction reaches equilibrium after 6 h. Interaction effects between variables may play a role in process optimisation, which is an important direction for future scale-up experimental studies.

3.4 Stability of catalysts

The stability and reusability of ACC600, as critical metrics for practical application, were evaluated through consecutive batch reactions under optimal conditions. To ensure reliability, each cycle included a standardised separation, washing and regeneration procedure and the conversion was determined in triplicate. Furthermore, the changes in the physicochemical properties of the catalyst, including sulfonic acid density, surface composition and pore structure, were quantitatively monitored across cycles to correlate the decline in activity with specific deactivation pathways. As shown in Fig. 4, after 10 consecutive reaction cycles, the conversion decreases from 97.5% to 79.0%, indicating excellent catalytic stability.

Although ACC600 has a lower sulfonic acid density than the carbon-based solid acid catalyst prepared *via* one-step sulfonation in our previous study,[7] it exhibits considerably higher stability. On the one hand, the rigid carbon framework of ACC600 is less likely to generate fragmented polycyclic aromatic hydrocarbons at high temperatures, thereby reducing the leaching of active groups; on the other hand, ACC600 has a large pore volume and specific surface area, resulting in a lower content of sulfonic acid groups per unit area.[32,36] Based on the model proposed in our previous study—specifically the relationship between the formation of sulfonic esters during repeated catalysis and catalyst structure—it can be inferred that ACC600 generates fewer sulfonic esters during repeated use.[21]

To further assess the intrinsic stability of ACC600 independent of catalyst loading level, reuse experiments were also conducted at a lower catalyst loading of 2 wt% (Fig. S1, SI). Under these conditions, the initial conversion of oleic acid was 83.5%. After five consecutive cycles, the conversion decreased to 67.2%, retaining 80.5% of its initial activity. This retention rate is comparable to that observed at 6 wt% loading (79.0% after 10 cycles), especially considering the lower initial conversion, indicating that the stability of ACC600 is not heavily dependent on the catalyst loading level and reflects the robust anchoring of sulfonic acid groups *via* C–C bonds.

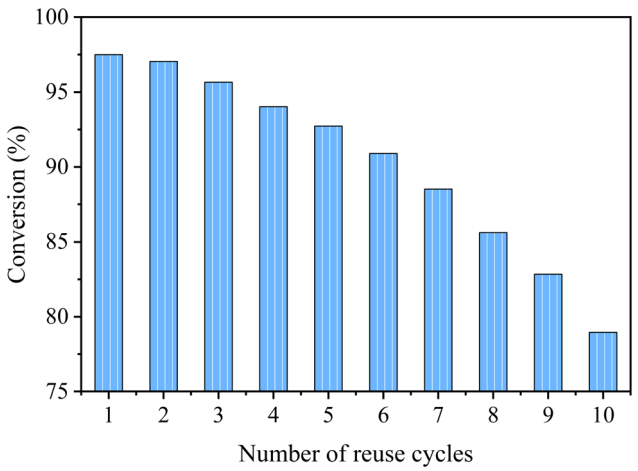

Fig. 4 Reusability of ACC600 in catalytic esterification reactions.

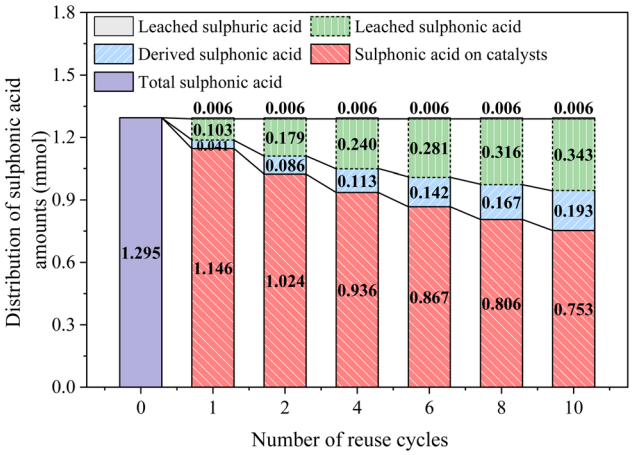

Fig. 5 Changes in sulfonic acid content during repeated catalytic esterification of oleic acid and methanol over ACC600.

To elucidate the stability mechanism of ACC600, we measured the sulfonic acid density and sulfur content on the surface of 1 g of ACC600 during reuse and analysed the change in the distribution of sulfonic acid groups based on the results of our previous study (Fig. 5).[21] The results show that after 10 reaction cycles, the sulfonic acid content of ACC600 decreases from 1.295 to 0.753 mmol. Among them, the content of sulfonated by-products containing sulfonic acid groups remaining on the catalyst surface is approximately 0.006 mmol and decreases to zero after the first reaction. The amount of leached sulfonic acid gradually increases with the number of reaction cycles: 0.103 mmol is leached after the first reaction and 0.343 mmol after the 10th reaction, accounting for 63.3% of the total sulfonic acid loss. In contrast, the amount of chemically derived sulfonic acid is relatively small, reaching 0.193 mmol after the 10th reaction. It suggests that the C–C bonded sulfonic acid sites are resistant to the formation of inactive derivatives, a common drawback of sulfonated carbons prepared by conventional methods. The above results indicate that ACC600 exhibits reduced leaching and chemical degradation of sulfonic acid groups, which extends the service life of the catalyst.

To further verify the reason for the enhanced stability of ACC600, the pore structure parameters of the catalyst before and after esterification reactions were measured (Table 4). The results show that the high specific surface area and well-developed pore structure of ACC600 provide highly dispersed anchoring sites and ample reaction space for sulfonic acid groups. This structure likely reduces the local concentration of active sites and alleviates diffusion limitations for reactants and products within the pore channels. Consequently, the structure of ACC600 minimises the leaching of sulfonic acid groups and side reactions caused by local supersaturation or mass transfer limitations, effectively extending the lifespan of the catalyst.

Table 4 Changes in the pore structure of ACC600 during repeated catalytic esterification reactions

Sample	Specific surface area ($m^2\ g^{-1}$)	Pore volume ($cm^3\ g^{-1}$)	Pore diameter (nm)
ACC600	627	0.71	5.57
ACC600 for 1 cycle	620	0.68	5.45
ACC600 for 2 cycles	618	0.69	5.40
ACC600 for 4 cycles	615	0.65	5.39

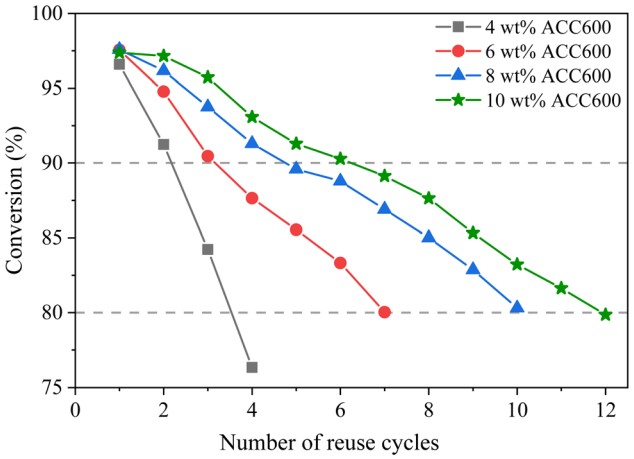

Fig. 7 Reusability of ACC600 in the esterification of soybean saponin acidified oil with methanol.

Our previous study has shown that the production of sulfonic esters is positively correlated with the concentration of sulfonic acid groups on the catalyst surface. Thus, increasing the specific surface area of the catalyst to reduce the concentration of surface sulfonic acid groups can inhibit the formation of sulfonic esters.[21]

Subsequently, the reused catalyst was characterised using XPS to analyse the changes in the content of sulfur-containing functional groups on its surface. As shown in Fig. 6, compared with the fresh catalyst, ACC600 reused for 4, 6, 8 and 10 cycles exhibits a characteristic peak at 167.4 eV in addition to the $-SO_3H$ peak at 168.6 eV. This peak corresponds to the presence of S–O linkages. Although the formation of specific sulfonic esters is challenging to distinguish solely based on XPS spectra, the appearance of this S–O component, combined with the concomitant quantitative decrease in $-SO_3H$ content (Fig. 5), strongly indicates the chemical transformation of sulfonic acid groups into derivatives such as sulfonic esters (R–O–SO_3H) or sulfonates.[37] With the increase in reuse cycles from 4 to 10, the proportion of S–O in the S 2p peak area increases from 40.6% to 51.2%, consistent with the results in Fig. 5.

To further assess the stability of the C–C bonded sulfonic acid sites, C 1s XPS spectra of used ACC600 were recorded (Fig. S2, SI). The relative proportion of the C–C component remained essentially unchanged throughout the reuse tests, indicating that the graphitic carbon backbone and the C–C linkages anchoring the sulfonic acid groups were not significantly degraded during the esterification reactions. This demonstrates that the C–C linkage not only prevents leaching but also preserves the active site structure, maintaining catalytic efficiency. The above results confirm that although the

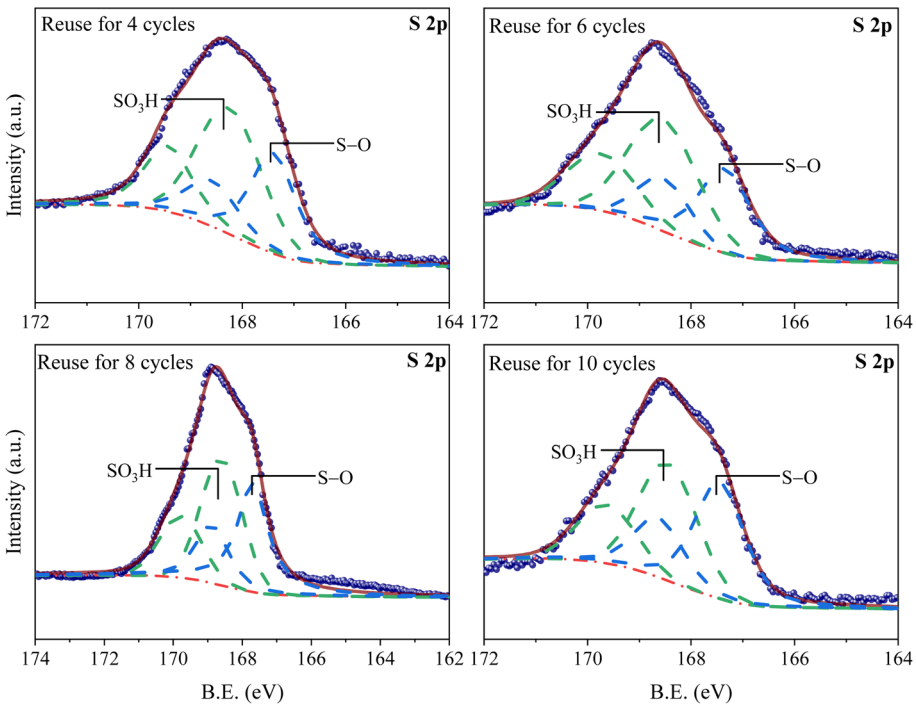

Fig. 6 S 2p XPS spectra of ACC600 throughout the repeated catalytic esterification of oleic acid and methanol.

Table 5 Comparison of the activity and stability of ACC600 with carbon-based solid acid catalysts reported in other studies

Catalyst precursor	Reaction conditions	Conversion (%)	Reusability (cycles, activity retention)	References
Coconut shell	Waste palm oil, 3 h, 130 °C	89.8	4, 77.5%	26
Sugarcane bagasse	Oleic acid, 6 h, 65 °C	87.0	4, 76.5%	38
Cocoa shell	Oleic acid, 24 h, 65 °C	77.0	4, 78%	39
Cellulose	Rapeseed oil fatty acids, 6 h, 65 °C	96.7	9, 80.2%	30
Corncob residue	Oleic acid, 8 h, 60 °C	86.5	3, 28.76%	40
Xanthoceras sorbifolia Bunge hulls	Acidified soybean soapstock, 5 h, 70 °C	97.2	4, 67.8%	19
Bamboo	Oleic acid, 8 h, 65 °C	98.0	5, 71.4%	7
Bamboo	Soybean saponin acidified oil, 6 h, 75 °C	98.1	12, 79.2%	This study

deactivation mechanism of the activated carbon-based solid acid catalyst is the same as that of conventional carbon-based solid acids, the combination of chemically robust C–C bonds and a physically rigid, high-surface-area carbon framework synergistically contributes to the long-term stability of the catalyst.

Finally, ACC600 with different loadings was used to catalyse the esterification of soybean saponin acidified oil (a practical feedstock for biodiesel production) under optimal conditions. As shown in Fig. 7, at a catalyst loading of 6 wt%, the conversion drops to nearly 80% after 7 reuse cycles. Although its reusability is inferior to that in the esterification of oleic acid under the same conditions, ACC600 still exhibits good catalytic stability. At the same time, the deactivation rate of the catalyst decreases with increasing catalyst loading. At catalyst loadings of 8 and 10 wt%, the conversion after the first reaction is close to 98%, decreasing to around 80% after 10 and 12 reuse cycles. Therefore, in the catalytic esterification of soybean saponin acidified oil, the catalyst loading can be appropriately increased to extend the number of reuse cycles while ensuring the normal progress of the reaction.

The performance of ACC600 was compared with that of representative carbon-based solid acid catalysts reported in recent literature for the esterification of oleic acid or similar high-FFA feedstocks (Table 5). Although many catalysts achieve high initial conversion (>90%), their reusability is often challenging, with a notable activity drop occurring within 3–5 cycles because of severe sulfonic group leaching. In contrast, ACC600 maintains 79.2% of its initial activity after 12 consecutive cycles. This superior stability was attributed to the unique combination of a rigid bamboo-activated carbon support and stable C–C bonding *via* aryldiazonium sulfonation, which effectively mitigated the two primary deactivation pathways.

Additionally, Table 6 presents the primary physicochemical properties of the biodiesel obtained through esterification. The results indicate that the physicochemical properties of ACC600-1 (biodiesel produced using ACC600 after one catalytic cycle) meet the ASTM D6751 standard in density, kinematic viscosity, acid value, moisture content, cetane number, flash point, ester content and sulfur content. This further confirms the excellent catalytic activity of ACC600.

Table 6 Main physicochemical properties of biodiesel produced from soybean saponin acidified oils

Physicochemical properties	ASTM D6751	ACC600-1
Density (20 °C)/(g cm^{-3})	0.82–0.9	0.85
Kinematic viscosity (40 °C)/(mm^2 s^{-1})	1.9–6.0	4.2
Acid value/(mg KOH per g)	<0.8	0.22
Moisture content/wt%	≤0.05	—
Cetane number	≥49	53
Flash point/°C	>130	135
Residual carbon/wt%	≤0.3	0.03
Ester content	>96.5	97.8
Sulfur content/(mg kg^{-1})	<5	—

4 Conclusion

Herein, a solid acid catalyst (ACC600) with high sulfonic acid density and excellent structural stability was prepared by grafting sulfonic acid groups onto bamboo-based activated carbon *via* the aryldiazonium sulfonation method. Under optimal preparation conditions (carbonisation temperature of 600 °C, sulfonating agent-to-activated carbon mass ratio of 10 : 1 and sulfonation time of 6 h), the catalyst showed a sulfonic acid density of 1.295 mmol g^{-1}, abundant pore structures and a high specific surface area, which facilitated the diffusion of reactants and the exposure of active sites. In the esterification reaction, ACC600 exhibited a conversion of 97.5% under mild conditions (catalyst dosage of 6 wt%, methanol/oil molar ratio of 6 : 1, reaction temperature of 75 °C and reaction time of 6 h) and outstanding reusability, retaining 79.0% of its initial catalytic activity after 10 consecutive reaction cycles. The excellent stability of ACC600 is attributed to the covalent attachment of –SO_3H groups *via* C–C bonds, which resist hydrolysis and leaching, combined with a rigid carbon framework with high surface area and well-developed porosity. This dual chemical–physical stabilization ensures the preservation of active sites during repeated esterification reactions. ACC600 also showed promising performance in the esterification of practical soybean saponin acidified oil, with an appropriate increase in

the catalyst loading found to prolong its service life. This work provides a theoretical basis and technical reference for the design of high-performance solid acid catalysts and their application in biodiesel production.

Conflicts of interest

There are no conflicts to declare.

Data availability

The data that support the findings of this study are available from the corresponding author up on reasonable request.

Supplementary information (SI) is available. See DOI: https://doi.org/10.1039/d5ra10105k.

Acknowledgements

The authors wish to acknowledge the financial support provided by the National Natural Science Foundation of China (52470137) & (52170121), and the National Environmental and Energy Base for International Science & Technology Cooperation.

References

1 A. Talebian-Kiakalaieh, N. A. S. Amin and H. Mazaheri, *Appl. Energy*, 2013, **104**, 683–710.
2 M. Hamza, M. Ayoub, R. Bin Shamsuddin, A. Mukhtar, S. Saqib, I. Zahid, M. Ameen, S. Ullah, A. G. Al-Sehemi and M. Ibrahim, *Environ. Technol. Innov.*, 2021, **21**, 101200.
3 H. Chebbi, D. Leiva-Candia, M. Carmona-Cabello, A. Jaouani and M. P. Dorado, *Ind. Crops Prod.*, 2019, **139**, 111535.
4 N. M. Daud, S. R. Sheikh Abdullah, H. Abu Hasan and Z. Yaakob, *Process Saf. Environ. Prot.*, 2015, **94**, 487–508.
5 I. M. Atadashi, M. K. Aroua, A. R. Abdul Aziz and N. M. N. Sulaiman, *Renew. Sustain. Energy Rev.*, 2012, **16**, 3275–3285.
6 M. X. Y. Ravindran, N. Asikin-Mijan, G. AbdulKareem-Alsultan, H. C. Ong, N. M.M, H. V Lee, T. A. Kurniawan, D. Derawi, S. F. M. Yusoff, I. M. Lokman and Y. H. Taufiq-Yap, *J. Environ. Chem. Eng.*, 2024, **12**, 112330.
7 B. Zhang, M. Gao, J. Geng, Y. Cheng, X. Wang, C. Wu, Q. Wang, S. Liu and S. M. Cheung, *Renewable Energy*, 2021, **164**, 824–832.
8 D. Shu, J. Zhang, R. Ruan, H. Lei, Y. Wang, Q. Moriko, R. Zou, E. Huo, D. Duan, L. Gan, D. Zhou, Y. Zhao and L. Dai, *Molecules*, 2024, **29**, 247.
9 B. Zhang, M. Gao, W. Tang, X. Wang, C. Wu and Q. Wang, *Energy Convers. Manag.*, 2023, **278**, 116708.
10 W. Miao, G. Fu, M. Fu, L. Xiang, T. Wang, T. Le, L. Zhang and P. D. Lenh, *Process Saf. Environ. Prot.*, 2025, **204**, 108138.
11 X. Liu, L. Zhang, W. Sun, M. Zhang and S. Yu, *Res. Chem. Intermed.*, 2017, **43**, 5917–5932.
12 L. J. Konwar, P. Mäki-Arvela and J. P. Mikkola, *Chem. Rev.*, 2019, **119**, 11576–11630.
13 J. M. Fonseca, L. Spessato, A. L. Cazetta, C. da Silva and V. d. C. Almeida, *Chem. Eng. Process. Process Intensif.*, 2021, **222**, 108668.
14 J. M. Anderson, R. L. Johnson, K. Schmidt-Rohr and B. H. Shanks, *Carbon*, 2014, **74**, 333–345.
15 A. H. Van Pelt, O. A. Simakova, S. M. Schimming, J. L. Ewbank, G. S. Foo, E. A. Pidko, E. J. M. Hensen and C. Sievers, *Carbon*, 2014, **77**, 143–154.
16 A. Mahajan and P. Gupta, *Environ. Chem. Lett.*, 2020, **18**, 299–314.
17 H. Pan, Q. Xia, Y. Wang, Z. Shen, H. Huang, Z. Ge, X. Li, J. He, X. Wang, L. Li and Y. Wang, *Fuel Process. Technol.*, 2022, **237**, 107421.
18 A. H. Noor Armylisas, S. S. Hoong, T. N. M. Tuan Ismail and C. H. Chan, *Waste Manag.*, 2024, **189**, 34–43.
19 F. Guo, Z. L. Xiu and Z. X. Liang, *Appl. Energy*, 2012, **98**, 47–52.
20 H. Yu, S. Niu, T. Bai, X. Tang and C. Lu, *J. Clean. Prod.*, 2018, **183**, 67–76.
21 B. Zhang, M. Gao, W. Tang, X. Wang, C. Wu, Q. Wang and H. Xie, *Energy*, 2023, **271**, 127079.
22 C. Yogin Soodesh, A. K. Seriyala, Navjot, P. Chattopadhyay, N. Rozhkova, B. Michalkiewicz, S. Chatterjee and B. Roy, *Chem. Eng. Res. Des.*, 2024, **203**, 759–788.
23 K. Saikia, A. Das, A. H. Sema, S. Basumatary, N. Shaemningwar Moyon, T. Mathimani and S. L. Rokhum, *Renewable Energy*, 2024, **229**, 120743.
24 S. Niu, Y. Ning, C. Lu, K. Han, H. Yu and Y. Zhou, *Energy Convers. Manag.*, 2018, **163**, 59–65.
25 E. Doustkhah, J. Lin, S. Rostamnia, C. Len, R. Luque, X. Luo, Y. Bando, K. C. W. Wu, J. Kim, Y. Yamauchi and Y. Ide, *Chem. – Eur J.*, 2019, **25**, 1614–1635.
26 I. Thushari, S. Babel and C. Samart, *Renewable Energy*, 2019, **134**, 125–134.
27 P. Dornath, S. Ruzycky, S. Pang, L. He, P. Dauenhauer and W. Fan, *Green Chem.*, 2016, **18**, 6637–6647.
28 B. Wu, S. Shen, S. Yuan, H. Pan, C. Wang, S. Jing, J. Li and Y. Zhao, *Mol. Catal.*, 2021, **506**, 111539.
29 D. Mao, X. Zhang, X. Zhang, M. Jia and J. Yao, *Chin. J. Chem. Eng.*, 2019, **27**, 1067–1072.
30 K. Malins, J. Brinks, V. Kampars and I. Malina, *Appl. Catal., A*, 2016, **519**, 99–106.
31 M. E. González, M. Cea, D. Reyes, L. Romero-Hermoso, P. Hidalgo, S. Meier, N. Benito and R. Navia, *Energy Convers. Manag.*, 2017, **137**, 165–173.
32 L. J. Konwar, P. Mäki-Arvela, E. Salminen, N. Kumar, A. J. Thakur, J. P. Mikkola and D. Deka, *Appl. Catal., B Environ.*, 2015, **176–177**, 20–35.
33 F. Liu, K. Huang, A. Zheng, F. S. Xiao and S. Dai, *ACS Catal.*, 2018, **8**, 372–391.
34 F. Javed, Z. Shamair, A. Hafeez, T. Fazal, R. Aslam, S. Akram, N. Rashid, W. B. Zimmerman and F. Rehman, *J. Clean. Prod.*, 2021, **311**, 127525.
35 L. J. Konwar, R. Das, A. J. Thakur, E. Salminen, P. Mäki-Arvela, N. Kumar, J. P. Mikkola and D. Deka, *J. Mol. Catal., A Chem.*, 2014, **388–389**, 167–176.

36 I. Thushari and S. Babel, *Bioresour. Technol.*, 2018, **248**, 199–203.
37 J. M. Fraile, E. García-Bordejé, E. Pires and L. Roldán, *J. Catal.*, 2015, **324**, 107–118.
38 K. P. Flores, J. L. O. Omega, L. K. Cabatingan, A. W. Go, R. C. Agapay and Y. H. Ju, *Renewable Energy*, 2019, **130**, 510–523.
39 C. M. Mendaros, A. W. Go, W. J. T. Nietes, B. E. J. O. Gollem and L. K. Cabatingan, *Renewable Energy*, 2020, **152**, 320–330.
40 S. Dechakhumwat, P. Hongmanorom, C. Thunyaratchatanon, S. M. Smith, S. Boonyuen and A. Luengnaruemitchai, *Renewable Energy*, 2020, **148**, 897–906.